ACS OMEGA

Article

Cite This: ACS Omega 2018, 3, 7655−7662

Facile Method to Prepare for the Ni_2P Nanostructures with Controlled Crystallinity and Morphology as Anode Materials of Lithium-Ion Batteries

Chungho Kim, Hyunhong Kim, Yonghoon Choi, Han Ah Lee, Yoon Seok Jung, and Jongnam Park*

School of Energy and Chemical Engineering, Ulsan National Institute of Science and Technology (UNIST), Ulsan 44919, Korea

Supporting Information

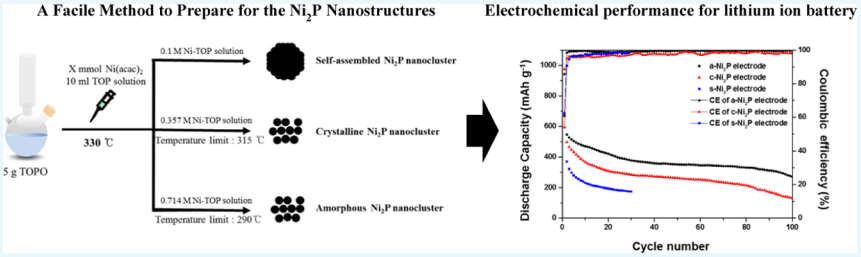

ABSTRACT: Conversion reaction materials (transition metal oxides, sulfides, phosphides, etc.) are attractive in the field of lithium-ion batteries because of their high theoretical capacity and low cost. However, the realization of these materials in lithium-ion batteries is impeded by large voltage hysteresis, high polarization, inferior cycle stability, rate capability, irreversible capacity loss in first cycling, and dramatic volume change during redox reactions. One method to overcome these problems is the introduction of amorphous materials. This work introduces a facile method to synthesize amorphous and crystalline dinickel phosphide (Ni_2P) nanoparticle clusters with identical morphology and presents a direct comparison of the two materials as anode materials for rechargeable lithium-ion batteries. To assess the effect of crystallinity and hierarchical structure of nanomaterials, it is crucial to conserve other factors including size, morphology, and ligand of nanoparticles. Although it is rarely studied about synthetic methods of well-controlled Ni_2P nanomaterials to meet the above criteria, we synthesized amorphous, crystalline Ni_2P, and self-assembled Ni_2P nanoparticle clusters via thermal decomposition of nickel−surfactant complex. Interestingly, simple modulation of the quantity of nickel acetylacetonate produced amorphous, crystalline, and self-assembled Ni_2P nanoparticles. A 0.357 M nickel−trioctylphosphine (TOP) solution leads to a reaction temperature limitation (∼315 °C) by the nickel precursor, and crystalline Ni_2P (c-Ni_2P) nanoparticles clusters are generated. On the contrary, a lower concentration (0.1 M) does not accompany a temperature limitation and hence high reaction temperature (330 °C) can be exploited for the self-assembly of Ni_2P (s-Ni_2P) nanoparticle clusters. Amorphous Ni_2P (a-Ni_2P) nanoparticle clusters are generated with a high concentration (0.714 M) of nickel−TOP solution and a temperature limitation (∼290 °C). The a-Ni_2P nanoparticle cluster electrode exhibits higher capacities and Coulombic efficiency than the electrode based on c-Ni_2P nanoparticle clusters. In addition, the amorphous structure of Ni_2P can reduce irreversible capacity and voltage hysteresis upon cycling. The amorphous morphology of Ni_2P also improves the rate capability, resulting in superior performance to those of c-Ni_2P nanoparticle clusters in terms of electrode performance.

1. INTRODUCTION

With global warming and fluctuating oil prices, research on new energy sources that are based on eco-friendly and abundant resources such as solar radiation, wind, and waves has become an important topic worldwide.[1−5] With these new energy sources, the importance of energy-storage devices is also gradually being recognized. In particular, lithium-ion batteries (LIBs) are promising power sources for not only cell phones and laptops but also electric vehicles and energy storage systems.[4−7] Many commercial LIBs consist of a $LiCoO_2$ cathode, a carbon anode, and a separator with an electrolyte.[8] To improve the current LIB performance, it is necessary to use new negative electrode materials which have high capacity, low cost, and environmental benignity.[6,9,10] Recently, a new reactivity concept based on the reversible electrochemical reaction of lithium is attracting attention in the field of LIBs.[11,12] In the conversion reaction, the active electrode is consumed by Li ions and converted to an embedded nanometer-scale metal in a lithium-anion matrix.[11−13] Conversion reaction materials have notable advantages, including high theoretical capacity because of transfer of more than one electron per 3D metal in a redox cycle. Good electronic conductivity from the Li−X matrix (X = O, F, N, S, and P) and short diffusion distance from the metal nanocomposite are also benefits.[7,11,12] However, conversion reaction materials have many drawbacks in terms of their use

Received: March 14, 2018
Accepted: June 15, 2018
Published: July 11, 2018

DOI: 10.1021/acsomega.8b00482
ACS Omega 2018, 3, 7655−7662

as negative electrode of LIBs. In particular, large polarization, irreversible capacity loss on first cycling, low Coulombic efficiency, extreme voltage hysteresis, volume expansion during the redox cycle, and poor kinetics have not yet been resolved.[11−13]

Successful strategies to overcome these problems include reducing the particle size of materials to the nanometer scale to accommodate large volume change[8,13−18] and using amorphous electrodes to replace crystalline materials to achieve faster conversion reaction rates.[19−24] Maier et al. reported enhanced potential of an amorphous RuO_2 electrode.[20] Zachariah et al. reported that interspersed amorphous MnO_x−carbon nanocomposites have superior electrochemical performance,[19] and Stevenson et al. demonstrated a great method to produce amorphous FeP_2 in high yield and remarkable performance.[21]

However, to the best of our knowledge, there is no report about pure difference between amorphous and crystalline electrodes except for other factors such as size differential, existence of conducting agent, different morphology, and so on. Our group has the curiosity for a pure amorphous effect on conversion reaction system under identical conditions.

Therefore, we are trying to introduce a facile method for synthesizing amorphous and crystalline dinickel phosphide nanoparticle clusters. Furthermore, the electrochemical difference of conversion reaction between crystalline and amorphous materials with Li^+ by using nickel phosphides was analyzed. Synthetic methods for nanoscale Ni_2P in different forms such as wires, solid particles, hollow particles, and rods were reported.[25−28] Research studies about sandwich-like-coupled Ni_2P nanoparticles and graphene were also studied.[29,30] In particular, amorphous nickel phosphide was introduced by Tracy group that amorphous-solid nickel phosphide forms at 240 °C under phosphine-rich condition.[31] In addition, Tu group made a core/shell-structured amorphous@crystalline nickel phosphide nanoparticles by ionothermal method.[22]

Herein, a facile method to synthesize Ni_2P nanostructures with controlled crystallinity and identical morphology by adjusting the quantity of nickel acetylacetonate is introduced. Furthermore, amorphous Ni_2P (a-Ni_2P) nanoparticle clusters were electrochemically compared with crystalline Ni_2P (c-Ni_2P) to unveil the amorphous effect on the conversion reaction with Li^+.

2. RESULTS AND DISCUSSION

Amorphous and crystalline Ni_2P nanoparticle clusters with identical morphology were synthesized by the thermal decomposition of metal surfactant complex, depending on the nickel precursor concentration. To obtain the nanostructured Ni_2P materials, we adopted the thermal decomposition method of metal−surfactant complex, which is superior to other synthetic routes in terms of control of size, morphology, and phase.[25] Using this method, we successfully synthesized the Ni_2P nanostructured anode materials with controlled morphology and crystallinity of Ni_2P nanomaterials by facile control of molar concentration of injected precursors. Figure 1 shows the X-ray diffraction patterns for the resulting a-Ni_2P, c-Ni_2P, and self-assembled Ni_2P (s-Ni_2P) nanoparticle clusters, respectively. Figure 1a has only a broad peak at about 45°, indicating that an amorphous material was synthesized. Transmission electron microscopy (TEM), scanning electron microscopy (SEM), and energy-dispersive spectroscopy (EDS)

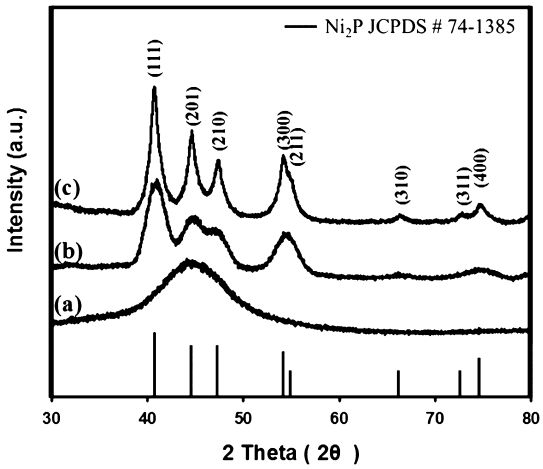

Figure 1. High-power XRD data of (a) amorphous Ni_2P nanoparticle clusters, (b) crystalline Ni_2P nanoparticle clusters, and (c) self-assembled Ni_2P nanoparticle clusters.

measurements were performed to verify that the sample (a) is Ni_2P. The X-ray diffractometer (XRD) patterns of c-Ni_2P nanoparticle clusters (Figure 1b) and s-Ni_2P nanoparticle clusters (Figure 1c) were perfectly matched with hexagonal nickel phosphide (JCPDS 74-1385). Broadening in the peaks of both particles implies the formation of nanometer scale particles. Furthermore, the diffraction peaks of s-Ni_2P nanoparticle clusters were stronger and sharper than those of c-Ni_2P nanoparticle clusters, indicating higher crystallinity.

Figure 2a,c shows TEM images of crystalline and amorphous Ni_2P nanoparticles clusters. Figure 2b,d clearly demonstrates that two types of nanoparticles have similar spherical morphology and size. The corresponding electron diffraction patterns of a-Ni_2P were smeared in one circle elucidating that the nanoparticles were amorphous (Figure S1). High-resolution TEM image of the c-Ni_2P showed the lattice fringe with the lattice spacing of 0.22 nm, which is corresponding to the (111) planes of hexagonal Ni_2P structure indicating the crystalline property (Figure S2). Each particle is on average 5 nm in diameter, and these small particles join together to form clusters. In addition, EDS measurements confirm that amorphous nanoparticle clusters are dinickel phosphides (Figure 2e). The ratio of components between nickel and phosphorus is almost 2:1. Cu and C come from the carbon-coated Cu substrate. Figure 3 illustrates the synthetic procedure. a-Ni_2P and c-Ni_2P electrodes that have identical morphology and size were prepared by injecting an Ni−trioctylphosphine (TOP) solution into TOP oxide (TOPO) as a bottom solution at 330 °C. The high temperature of the bottom solution leads to instantaneous formation of nuclei, followed by slow growth.[33] As a result, Ni_2P nanoparticles are formed. The synthetic mechanism of nickel phosphides is very well-known.[25,26,34] Our group previously reported that TOP is a good phosphorus source precursor to synthesize transition-metal phosphides.[26,35] Because C−P bonds in TOP catalytically are cleaved when combined with some metals, P atoms can diffuse into the metal,[36] thereby generating metal phosphides. a-Ni_2P, c-Ni_2P, and s-Ni_2P nanoparticle clusters are generated by adjusting the quantity of nickel acetylacetonate, which made it possible to limit the aging temperature. All syntheses are conducted under a TOP-rich condition in comparison with other experiments[25,31,37] because a TOP-rich

DOI: 10.1021/acsomega.8b00482
ACS Omega 2018, 3, 7655−7662

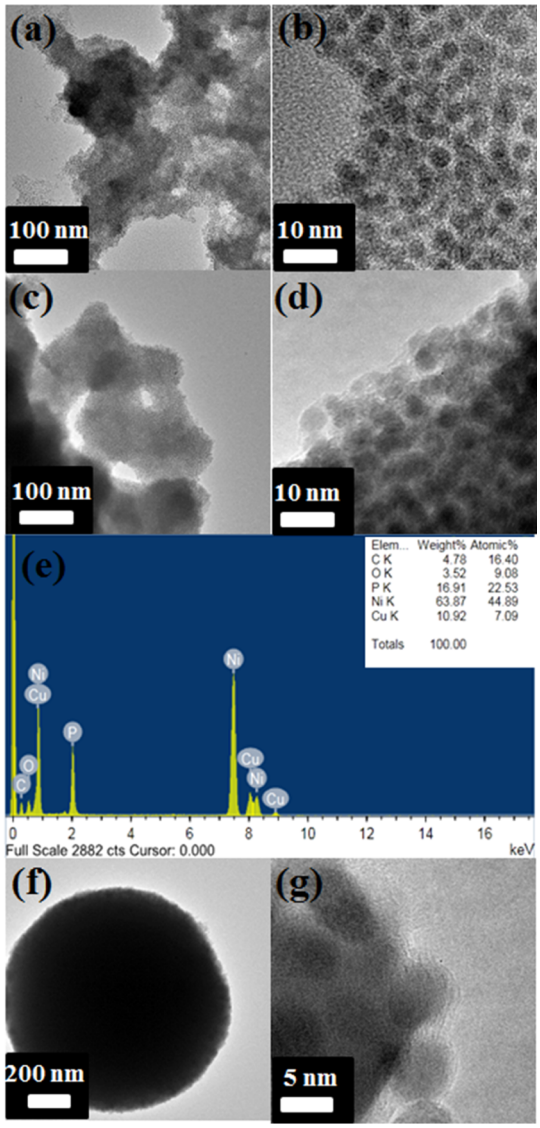

Figure 2. Normal TEM image of (a,b) crystalline Ni_2P nanoparticle clusters; (c,d) amorphous Ni_2P nanoparticle clusters; (e) EDS data of amorphous Ni_2P nanoparticle clusters; and (f,g) self-assembled Ni_2P nanoparticle clusters.

environment acts not only as a P source but also as a surfactant.

When the volume of Ni−TOP solution is based on 10 mL, 0.357 M Ni−TOP solution limits the reaction temperature (~315 °C) by the high concentration of the nickel precursor, and c-Ni_2P nanoparticle clusters are then generated. When the concentration of Ni−TOP solution is higher than 0. 714 M, a-Ni_2P nanoparticle clusters are formed because of the low reaction temperature (~290 °C) by the nickel precursor. Low aging temperature (below 300 °C) leads to amorphous Ni_2P nanoparticles[31] and a large amount of undecomposed TOP causes the nanoparticles to cluster.

Furthermore, a lower concentration (0.1 M) does not impose a temperature limitation, and hence high reaction temperature (330 °C) leads to the formation of s-Ni_2P nanoparticle clusters (Figure 2e). From the result of low volume/high concentration experiments, the reaction temperature has a dominant effect on shape control of crystalline Ni_2P over the injection solution concentration. The quantity of nickel precursor was fixed at 0.5 mmol, and the amount of TOP was reduced to 5, 2, and 1 mL. As the amount was decreased, the self-assembled spherical morphology collapsed (Figure S3).

2.1. Electrochemical Properties. Electrochemical measurements were performed on a 2016 coin-type half-cell, where Li metal foil was used as the counter electrode. Figure 4a shows the cycling performance of the Ni_2P electrodes at 0.5 C, and Figure 4b describes the rate performance of the Ni_2P electrodes. The first discharge capacities of a-Ni_2P and c-Ni_2P electrodes were 942.6 and 974.9 mA h g^{-1}, and the reversible charge capacities were 573.2 and 526.8 mA h g^{-1}, respectively. The higher capacities over the theoretical capacity (542 mA h g^{-1}) in the first cycle are related to decomposition of the electrolyte upon reduction with the formation of a polymeric film at low potentials and interfacial storage of Li^+.[11−13] Additionally, the a-Ni_2P electrodes exhibited better cycle result compared to c-Ni_2P electrodes. This result means that the isotropic environment and the absence of grain boundaries of amorphous structure relieve the damage during the insertion of lithium ion.[39] In the subsequent cycles, the a-Ni_2P electrode showed better Coulombic efficiency (99.1%) and capacity retention than the c-Ni_2P electrode (96.8%). Furthermore, reversible capacities of the two forms of Ni_2P after 50 cycles were 351.5 and 262.9 mA h g^{-1}. In Figure 4b, the rate performance of a-Ni_2P nanoparticles is higher than c-Ni_2P, and it means that diffusion of lithium ion in a-Ni_2P nanoparticles is superior to c-Ni_2P.[40] According to previous studies, it has been suggested that percolation pathways from interfacial region in disordered structure increase the Li diffusivity.[41] The reason for enhancement is an increase of pre-exponential factors and/or a decrease of the activation energy of the Arrhenius equation.[42] One of the products, s-Ni_2P nanoclusters, was also

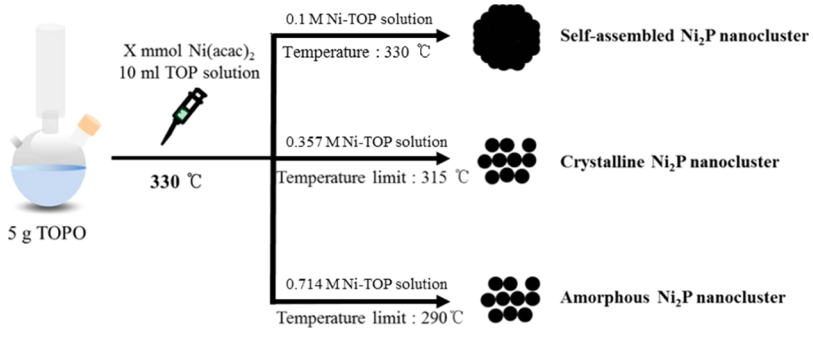

Figure 3. Schematic illustration of the formation of nickel phosphides.

DOI: 10.1021/acsomega.8b00482
ACS Omega 2018, 3, 7655−7662

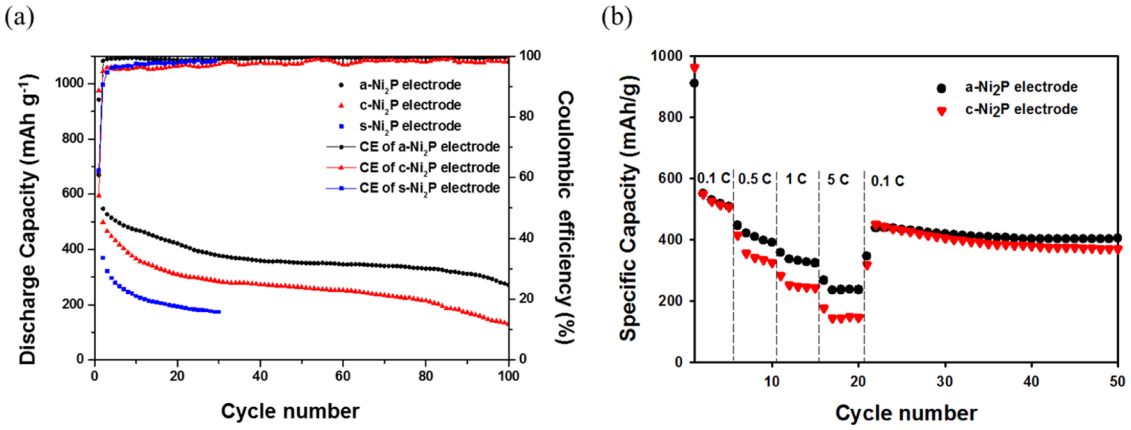

Figure 4. (a) Cyclic performance of Ni_2P nanoparticles cluster electrodes at 0.5 C. (b) Rate performance of a-Ni_2P and c-Ni_2P nanoparticle cluster electrodes.

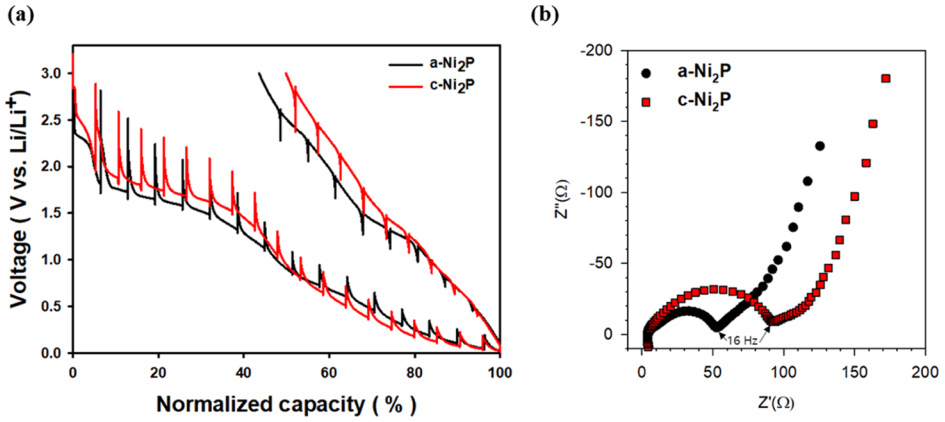

Figure 5. (a) GITT curves of both electrodes in the first cycle and (b) Nyquist plots for electrodes of a-Ni_2P nanoparticles and c-Ni_2P nanoparticles.

studied because it is well-established that self-assembled structures have the potential to reduce the transport pathways of Li^+ ions and electrons.[50] To confirm the effect of secondary hierarchical Ni_2P structures, we evaluated its cycle performance and electrochemical impedance spectroscopy (EIS) measurement (Figure S4). However, its specific capacity (174 mA h g^{-1} after 30 cycles) was significantly lower than the theoretical capacity (542 mA h g^{-1}); we thought that significant side reactions would be dominant in this case compared to a-Ni_2P and c-Ni_2P nanoparticles. The cell performance of a-Ni_2P nanoparticles (351.5 mA h g^{-1}) can be matched with other type of Ni_2P electrodes. Porous Ni_2P nanosheets, single crystalline Ni_2P nanowires, and hierarchical Ni_2P spheres presented the reversible capacities of 379.8, 326, and 365.3 mA h g^{-1} respectively at 0.5 C after 50 cycles.[16,46,48] Comparing to the amorphous anode electrode, the performance of c-Ni_2P (262.9 mA h g^{-1}) was significantly lower than other structured Ni_2P electrodes.

The gap in the initial reversible capacity was continuously maintained throughout the cycling. In other words, the initial Coulombic efficiency (ICE) is very important in conversion reaction electrodes. The gap in the ICE between the two nickel phosphide electrodes proves that a-Ni_2P is superior to c-Ni_2P at the first cycle. The a-Ni_2P nanoparticle cluster electrode has a higher ICE (average 63.61%) than the c-Ni_2P nanoparticle cluster electrode (average 58.20%) at 0.1 C, and the same results were obtained at 0.5 C (Figure S5). The irreversible capacity loss upon the first cycle is from the formation of a solid electrolyte interphase (SEI) layer and irreversible conversion reaction.[11,12] To shed light on this irreversible capacity gap of both electrodes upon first cycling, we analyze both electrodes by the galvanostatic intermittent titration technique (GITT). The GITT is one of the most powerful techniques for observing key thermodynamics and kinetic data about battery performance.[49] Figure 5a shows the GITT curves of the two electrodes. The relaxation time is 4 h. It is well-known that upon first cycling, nickel phosphides convert to Li_3P and Ni with an intermediate step of an insertion reaction.[14,16] In the initial normalized capacity region, the plateau indicates that Ni_2P forms intermediate Li_x−Ni_2P by an insertion reaction because of the covalence of nickel phosphides. Another plateau represents the conversion process where Li_x−Ni_2P and lithium convert to a Li_3P matrix and nickel metal.[14] The advantage of a-Ni_2P in electrical networking was confirmed by EIS measurements (Figure 5b). By comparing the result of c-Ni_2P electrodes, the spectra for a-Ni_2P electrodes exhibit much smaller high-frequency semicircle which is interpreted by enhanced electronic conductivity and charge-transfer kinetics of the a-Ni_2P networking. The polarization between closed-circuit voltage and quasi-open-circuit voltage (QOCV) after 4 h relaxation at the first cycling is indicated in Figure S6. In the initial discharge region, polarization of a-Ni_2P was higher than that of c-Ni_2P. However, the polarization reversed during the

DOI: 10.1021/acsomega.8b00482
ACS Omega 2018, 3, 7655−7662

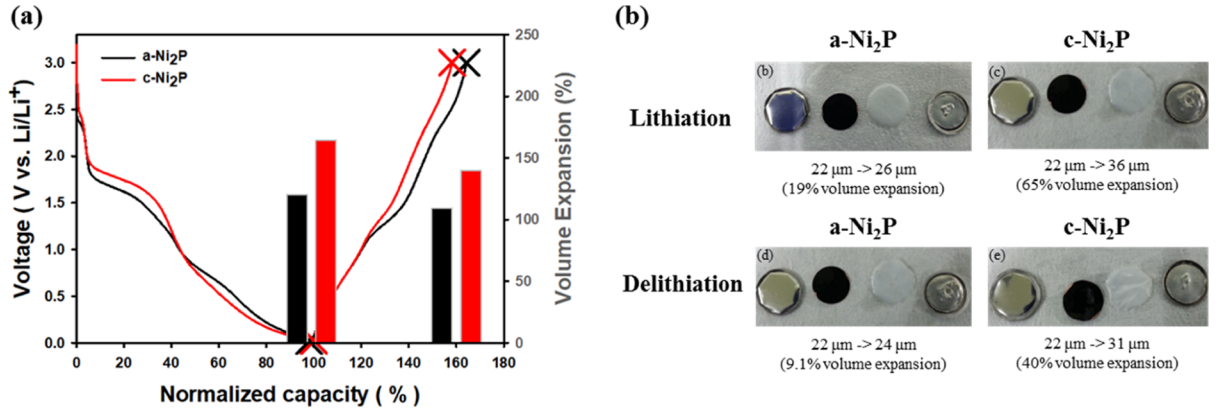

Figure 6. (a) Voltage profiles (solid line) of Ni_2P nanoparticle cluster electrodes and the corresponding electrode thickness change (bar) during lithiation and delithiation. (b) Camera image of opened electrodes after cycling: a-Ni_2P nanoparticles and c-Ni_2P nanoparticles during lithiation and delithiation.

discharge process. The polarization can represent the resistance by the equation $V = IR$ because the current is constant. Therefore, the results indicate that the resistances of both electrodes were reversed in the middle of the reaction. This reversal of resistance is due to the additional resistance under amorphization of the c-Ni_2P electrode. Amorphous electrodes can react with lithium as solid solution behavior without a phase transition.[43] Therefore, the a-Ni_2P electrode has reduced resistance because the loss of electrical contact between particles during the conversion reaction by large volume changes and structural stresses are reduced. After the region of insertion process, the polarization of both electrodes sharply decreases in the first discharge process because Ni_2P converts to a Ni/Li_3P complex, which has good electronic conductivity by the way of conversion process.[44]

The large voltage hysteresis is one of the features of the conversion process.[14] Comparing the electrodes, the a-Ni_2P electrode has lower voltage hysteresis than the c-Ni_2P electrode for the conversion reaction between the first lithiation and delithiation process (Figure S7a). This is a critical factor to improve the ICE of the conversion process.[14] Furthermore, the gap of the voltage hysteresis between the two electrodes is continuously maintained throughout cycling. The voltage hysteresis curve between the first charge and the second discharge profile (Figure S7b) and the gap of QOCV from the GITT curve also indicated that a-Ni_2P has lower voltage hysteresis than c-Ni_2P. This is ascribed, at least in part, to amorphization of crystalline Ni_2P, which has enhanced Gibbs free energy.[19,20] The above results suggest that a-Ni_2P may achieve a faster conversion reaction and lower volume expansion than the c-Ni_2P electrode.[19] This is a very interesting result because large voltage hysteresis between charge and discharge is a major to commercialize conversion materials because of the diminished round-trip efficiency of the electrode.[14]

The volume expansion of electrodes during lithiation and delithiation was measured through ex situ measurement of electrode thickness (Figure 6). All cells were cycled for 0.1 C at 30 °C in a potential range of 0.02−3.0 V versus Li/Li^+. After full lithiation until the redox potential of the working electrode reached 0.02 V versus Li/Li^+, the c-Ni_2P and a-Ni_2P electrodes led to considerably smaller volume expansion than the theoretical volume expansion because the nanostructure reduces the mechanical strain induced by volume change.[15,38,45] In addition, the a-Ni_2P electrode showed considerable volume expansion of about 120%, whereas the c-Ni_2P electrode displayed a thickness change of about 164% in the fully lithiated state. As shown in SEM data (Figure S8), we could detect more heterogeneous region on c-Ni_2P electrodes compared with a-Ni_2P electrodes. A tendency to agglomerate between s-Ni_2P nanoclusters after cycling in SEM image was observed because high crystallinity is unfavorable to relieve the damage during insertion of lithium ion (Figure S9). As the cycle processed, the contact between c-Ni_2P and binder was rapidly deteriorated, and this might interrupt the migration of electrons in electrodes.

Figure S10 shows the electrochemical behavior of the a-Ni_2P and c-Ni_2P nanoparticle cluster electrodes characterized by cyclic voltammograms at a scanning rate of 0.2 mV s^{-1} between 0.02 and 3 V. The small anodic peak of a-Ni_2P at 1.80 V implies that Ni_2P reacts with Li^+ by an insertion process. The maximum reduction peak of a-Ni_2P is located at 0.66 V. The maximum peak indicates that Li_x−Ni_2P decomposes to not only metallic Ni and a Li_3P matrix but also forms of the SEI layer.[16,46] For c-Ni_2P, these peaks shift to 1.93 and 0.94 V. Comparing the intensity of redox peaks of both electrodes, the peaks of the a-Ni_2P electrode are sharper than those of c-Ni_2P. In particular, the second oxidation peak of the a-Ni_2P electrode, which is evidently higher than the others, suggests that the amount of reversible reaction is larger than that of the c-Ni_2P electrode.[16,47]

3. CONCLUSIONS

Crystalline and amorphous nickel diphosphide nanoparticle clusters that have almost same shape and size were synthesized by a simple hot-injection method. This was achieved by adjusting the quantity of nickel acetylacetonate, which made it possible to limit the aging temperature. Furthermore, its electrochemical characteristics were investigated to analyze the effect of amorphous morphology on the conversion reaction in a LIB. These materials were characterized by TEM, SEM, XRD, and EDS. From the characterization, amorphous and crystalline spherical ∼5 nm clusters have almost the same size and structure. In addition, self-assembled Ni_2P nanoparticle clusters could be generated at 330 °C without oleylamine. The electrochemical results showed that amorphous materials in isolation from other factors can be used to overcome the problems impeding conversion reaction materials, such as low

DOI: 10.1021/acsomega.8b00482
ACS Omega 2018, 3, 7655−7662

ICE, large voltage hysteresis, capacity retention, and serious volume expansion. a-Ni_2P provides superior ICE over the crystalline materials in the conversion reaction with Li^+ because there is no amorphization process. In addition, amorphous nickel phosphide can reduce voltage hysteresis and volume expansion during cycling, which are very serious obstacles to the commercialization of conversion materials. In the future, it will be of significant interest to synthesize amorphous nanometer scale conversion materials such as iron oxides and manganese oxides.

4. EXPERIMENTAL SECTION

4.1. Materials. Nickel(II) acetylacetonate anhydrous [$Ni(acac)_2$] 95% was purchased from Strem Chemical Inc. TOP, technical grade, 90% and TOPO, technical grade, 90% were purchased from Sigma-Aldrich Co. LLC. Chloroform and ethanol were purchased from SK Chemical. All chemicals were used without further purification.

4.2. Synthesis of Nanosized Ni_2P Particles. The Ni_2P materials were synthesized by a hot-injection method in an argon atmosphere using standard Schlenk-line techniques. The s-Ni_2P was prepared by the following procedure. A Ni−TOP solution was prepared by reacting 1 mmol of $Ni(acac)_2$ and 10 mL of TOP (0.1 M Ni−TOP) at 60 °C until the solution became sky blue. A TOPO solution was also prepared by vigorous stirring at 330 °C. The Ni−TOP solution was added to 5 g of TOPO solution at once, and then the complex solution was maintained for 30 min. The reaction was stopped by cooling to room temperature. The nanoparticles were isolated by the addition of 30 mL of ethanol and 5 mL of chloroform, followed by centrifugation. The c-Ni_2P nanoparticles were synthesized by injecting a 0.357 M Ni−TOP solution to a TOPO solution, prepared by stirring at 330 °C. Then, the reaction was kept for 30 min. The temperature was increased up to 315 °C because of the endothermic reaction and washed with ethanol by centrifugation. The a-Ni_2P nanoparticles were synthesized by injecting a 0.714 M Ni−TOP solution to a TOPO solution prepared by stirring at 330 °C. Then, the reaction was maintained for 30 min. The temperature was limited to 290 °C because of the endothermic reaction of precursors and the nanoparticles were washed with ethanol by centrifugation.

4.3. Characterization. Powder XRD data were collected on a D/MAZX 2500V/PC (Rigaku) using Cu Kα radiation (λ = 0.15405 nm), operated for 2θ = 10−80° with a scan rate = 2°/min. The material morphology was examined using a field-emission TEM (JEOL JEM-2100) operated at 200 kV and a cold field-emission SEM (Hitachi s-4800). After cycling, cells were disassembled at an atmosphere environment to observe changes of thickness of electrodes. The electrodes were washed several times with dimethyl carbonate (DMC) to remove electrolyte and dried for ex situ measurement. The thickness of five randomly selected points of dried electrodes was measured by Vernier calipers.[32] This ex situ measurement was proved to be an efficient way to estimate the change of volume, easily verifying the volume change behavior. For ex situ SEM, the cells were disassembled after 23 cycles in Ar-filled glovebox and then washed by DMC.

4.4. Electrochemical Investigation. Electrochemical measurements were performed on a 2016 coin-type half cell, where Li metal foil was used as the counter electrode. The working electrodes were fabricated using a mixture of active materials (75 wt %), super P (15 wt %), and polyvinylidene fluoride binder (LG Chem. 10%) in *N*-methylpyrrolidinone. The electrolyte was 1.3 M $LiPF_6$ in a 3:7 volume mixture of ethylene carbonate and diethyl carbonate, and a microporous polyethylene film was used as a separator. The weight of the anode materials was measured as ∼0.9 mg for each cell. Cells were assembled in an Ar-filled glovebox with less than 1 ppm of both oxygen and moisture. Galvanostatic charge and discharge cycling (WonATech WBCS 3000 battery measurement system) was performed in a potential window from 0.02 to 3.0 V versus Li/Li^+ at current densities from 0.1 to 5 C. The EIS was measured from 1.5 MHz to 5 mHz with an amplitude of 10 mV. The half-cells were discharged to 0.4 V (vs Li/Li^+) at 270 mA g^{-1}, and a constant voltage of 0.4 V was applied until the current decreased to 27 mA g^{-1}. Then, the cells were allowed to rest for 3 h. Cyclic voltammograms were performed at a scanning rate of 0.2 mV s^{-1} between 0.02 and 3 V using an SP150 potentiostat (BioLogic Science Instruments) with homemade three-electrode cells.

■ ASSOCIATED CONTENT

Supporting Information

The Supporting Information is available free of charge on the ACS Publications website at DOI: 10.1021/acsomega.8b00482.

SEM image of s-Ni_2P nanoparticles clusters by concentration of Ni−TOP solution; charge and discharge capacities of Ni_2P nanoparticles cluster electrodes at 0.5 C; voltage difference from GITT curve between close-circuit voltage and open-circuit voltage on first discharge and charge process; voltage hysteresis curve between first charge and second discharge profile and first cycle and second discharge curve of nickel phosphide electrodes; and rate performance of a-Ni_2P and s-Ni_2P nanoparticles cluster electrodes (PDF)

■ AUTHOR INFORMATION

Corresponding Author

*E-mail: jnpark@unist.ac.kr.

ORCID

Yoon Seok Jung: 0000-0003-0357-9508

Jongnam Park: 0000-0002-0954-0172

Author Contributions

C.K. and H.K. contributed equally to this work. The manuscript was written through contributions of all authors. All authors have given approval to the final version of the manuscript. J.P. designed the project. J.P. and C.K. wrote the paper. C.K. and H.K. synthesized the nanomaterials, performed the LIB experiments, and analyzed the data. Y.C. developed the experimental setup for the synthesis of nanomaterials.

Notes

The authors declare no competing financial interest.

■ ACKNOWLEDGMENTS

This work was supported by the Basic Science Research Program through the National Research Foundation of Korea (NRF) funded by the Ministry of Education, (NRF-2015R 1D 1A 1A 01060843) and also supported by the brand research fund of the UNIST (1.160097.01/2V05120).

DOI: 10.1021/acsomega.8b00482
ACS Omega 2018, 3, 7655−7662

ABBREVIATIONS

Ni_2P, dinickel phosphine; LIBs, Lithium-ion batteries; Ni(acac)$_2$, Nickel(II) acetylacetonate anhydrous; TOP, trioctylphosphine; TOPO, trioctylphosphine oxide; DMC, dimethyl carbonate; XRD, X-ray diffractometer; TEM, transmission electron microscopy; SEM, scanning electron microscopy; EDS, energy-dispersive spectroscopy; SEI, solid electrolyte interphase; EIS, electrochemical impedance spectroscopy; GITT, galvanostatic intermittent titration technique; QOCV, quasi-open-circuit voltage

REFERENCES

(1) Hoffert, M. I.; Caldeira, K.; Benford, G.; Criswell, D. R.; Green, C.; Herzog, H.; Jain, A. K.; Kheshgi, H. S.; Lackner, K. S.; Lewis, J. S.; et al. Advanced Technology Paths to Global Climate Stability: Energy for a Greenhouse Planet. *Science* **2002**, *298*, 981−987.

(2) Guo, K. W. Green Nanotechnology of Trends in Future Energy. *Recent Pat. Nanotechnol.* **2011**, *5*, 76−88.

(3) Midilli, A.; Dincer, I.; Ay, M. Green Energy Strategies for Sustainable Development. *Energy Policy* **2006**, *34*, 3623−3633.

(4) Palacín, M. R. Recent Advances in Rechargeable Battery Materials: A Chemists Perspective. *Chem. Soc. Rev.* **2009**, *38*, 2565−2575.

(5) Goodenough, J. B.; Kim, Y. Challenges for Rechargeable Li Batteries. *Chem. Mater.* **2010**, *22*, 587−603.

(6) Marom, R.; Amalraj, S. F.; Leifer, N.; Jacob, D.; Aurbach, D. A Review of Advanced and Practical Lithium Battery Materials. *J. Mater. Chem.* **2011**, *21*, 9938.

(7) Cheng, F.; Liang, J.; Tao, Z.; Chen, J. Functional Materials for Rechargeable Batteries. *Adv. Mater.* **2011**, *23*, 1695−1715.

(8) Aricò, A. S.; Bruce, P.; Scrosati, B.; Tarascon, J.-M.; van Schalkwijk, W. Nanostructured Materials for Advanced Energy Conversion and Storage Devices. *Nat. Mater.* **2005**, *4*, 366−377.

(9) Liu, C.; Li, F.; Ma, L.-P.; Cheng, H.-M. Advanced Materials for Energy Storage. *Adv. Mater.* **2010**, *22*, E28−E62.

(10) Scrosati, B. Recent Advances in Lithium Ion Battery Materials. *Electrochim. Acta* **2000**, *45*, 2461−2466.

(11) Malini, R.; Uma, U.; Sheela, T.; Ganesan, M.; Renganathan, N. G. Conversion Reactions: A New Pathway to Realise Energy in Lithium-Ion Battery—Review. *Ionics* **2009**, *15*, 301−307.

(12) Cabana, J.; Monconduit, L.; Larcher, D.; Palacín, M. R. Beyond Intercalation-Based Li-Ion Batteries: The State of the Art and Challenges of Electrode Materials Reacting Through Conversion Reactions. *Adv. Energy Mater.* **2010**, *22*, E170−E192.

(13) Boyanov, S.; Annou, K.; Villevieille, C.; Pelosi, M.; Zitoun, D.; Monconduit, L. Nanostructured Transition Metal Phosphide as Negative Electrode for Lithium-Ion Batteries. *Ionics* **2008**, *14*, 183−190.

(14) Lu, Y.; Tu, J.-P.; Xiong, Q.-Q.; Qiao, Y.-Q.; Wang, X.-L.; Gu, C.-D.; Mao, S. X. Synthesis of Dinickel Phosphide (Ni_2P) for Fast Lithium-Ion Transportation: a New Class of Nanowires with Exceptionally Improved Electrochemical Performance as a Negative Electrode. *RSC Adv.* **2012**, *2*, 3430−3436.

(15) Jang, B.; Park, M.; Chae, O. B.; Park, S.; Kim, Y.; Oh, S. M.; Piao, Y.; Hyeon, T. Direct Synthesis of Self-Assembled Rerrite/carbon Hybrid Nanosheets for High Performance Lithium-Ion Battery Anodes. *J. Am. Chem. Soc.* **2012**, *134*, 15010−15015.

(16) Xu, X.; Cao, R.; Jeong, S.; Cho, J. Spindle-like Mesoporous α-Fe_2O_3 Anode Material Prepared from MOF Template for High-Rate Lithium Batteries. *Nano Lett.* **2012**, *12*, 4988−4991.

(17) Xia, H.; Xia, Q.; Lin, B.; Zhu, J.; Seo, J. K.; Meng, Y. S. Self-standing porous LiMn2O4 nanowall arrays as promising cathodes for advanced 3D microbatteries and flexible lithium-ion batteries. *Nano Energy* **2016**, *22*, 475−482.

(18) Jabeen, N.; Hussain, A.; Xia, Q.; Sun, S.; Zhu, J.; Xia, H. High-Performance 2.6 V Aqueous Asymmetric Supercapacitors based on In Situ Formed Na0.5MnO2 Nanosheet Assembled Nanowall Arrays. *Adv. Mater.* **2017**, *29*, 1700804.

(19) Guo, J.; Liu, Q.; Wang, C.; Zachariah, M. R. Interdispersed Amorphous MnO_x−Carbon Nanocomposites with Superior Electrochemical Performance as Lithium-Storage Material. *Adv. Funct. Mater.* **2012**, *22*, 803−811.

(20) Delmer, O.; Balaya, P.; Kienle, L.; Maier, J. Enhanced Potential of Amorphous Electrode Materials: Case Study of RuO_2. *Adv. Mater.* **2008**, *20*, 501−505.

(21) Hall, J. W.; Membreno, N.; Wu, J.; Celio, H.; Jones, R. A.; Stevenson, K. J. Low-Temperature Synthesis of Amorphous FeP_2 and Its Use as Anodes for Li Ion Batteries. *J. Am. Chem. Soc.* **2012**, *134*, 5532−5535.

(22) Zhang, H.; Lu, Y.; Gu, C.-D.; Wang, X.-L.; Tu, J.-P. Ionothermal Synthesis and Lithium Storage Performance of Core/shell Structured Amorphous@ Crystalline Ni−P nanoparticles. *CrystEngComm* **2012**, *14*, 7942−7950.

(23) Liu, P.; Hao, Q.; Xia, X.; Lei, W.; Xia, H.; Chen, Z.; Wang, X. Hollow Amorphous MnSnO3 Nanohybrid with Nitrogen-Doped Graphene for High-Performance Lithium Storage. *Electrochim. Acta* **2016**, *214*, 1−10.

(24) Liu, J.; Zheng, M.; Shi, X.; Zeng, H.; Xia, H. Amorphous FeOOH Quantum Dots Assembled Mesoporous Film Anchored on Graphene Nanosheets with Superior Electrochemical Performance for Supercapacitors. *Adv. Funct. Mater.* **2016**, *26*, 919−930.

(25) Muthuswamy, E.; Savithra, G. H. L.; Brock, S. L. Synthetic Levers Enabling Independent Control of Phase, Size, and Morphology in Nickel Phosphide Nanoparticles. *ACS Nano* **2011**, *5*, 2402−2411.

(26) Park, J.; Koo, B.; Yoon, K. Y.; Hwang, Y.; Kang, M.; Park, J.-G.; Hyeon, T. Generalized Synthesis of Metal Phosphide Nanorods via Thermal Decomposition of Continuously Delivered Metal− Phosphine Complexes Using a Syringe Pump. *J. Am. Chem. Soc.* **2005**, *127*, 8433−8440.

(27) Hu, X.; Yu, J. C. High-Yield Synthesis of Nickel and Nickel Phosphide Nanowires via Microwave-Assisted Processes. *Chem. Mater.* **2008**, *20*, 6743−6749.

(28) Henkes, A. E.; Vasquez, Y.; Schaak, R. E. Converting Metals into Phosphides: A General Strategy for the Synthesis of Metal Phosphide Nanocrystals. *J. Am. Chem. Soc.* **2007**, *129*, 1896−1897.

(29) Feng, Y.; Zhang, H.; Mu, Y.; Li, W.; Sun, J.; Wu, K.; Wang, Y. Monodisperse Sandwich-Like Coupled Quasi-Graphene Sheets Encapsulating Ni2P Nanoparticles for Enhanced Lithium-Ion Batteries. *Chem.—Eur. J.* **2015**, *21*, 9229−9235.

(30) Lu, Y.; Wang, X.; Mai, Y.; Xiang, J.; Zhang, H.; Li, L.; Gu, C.; Tu, J.; Mao, S. X. Ni2P/Graphene Sheets as Anode Materials with Enhanced Electrochemical Properties versus Lithium. *J. Phys. Chem. C* **2012**, *116*, 22217−22225.

(31) Wang, J.; Johnston-Peck, A. C.; Tracy, J. B. Nickel Phosphide Nanoparticles with Hollow, Solid, and Amorphous Structures. *Chem. Mater.* **2009**, *21*, 4462−4467.

(32) Park, Y.; Choi, N.-S.; Park, S.; Woo, S. H.; Sim, S.; Jang, B. Y.; Oh, S. M.; Park, S.; Cho, J.; Lee, K. T. Si-Encapsulating Hollow Carbon Electrodes via Electroless Etching for Lithium-Ion Batteries. *Adv. Energy Mater.* **2013**, *3*, 206−212.

(33) de Mello Donegá, C.; Liljeroth, P.; Vanmaekelbergh, D. Physicochemical Evaluation of the Hot-injection Method, a Synthesis Route for Monodisperse Nanocrystals. *Small* **2005**, *1*, 1152−1162.

(34) Chen, Y.; She, H.; Luo, X.; Yue, G.-H.; Peng, D.-L. Solution-phase Synthesis of Nickel Phosphide Single-crystalline Nanowires. *J. Cryst. Growth* **2009**, *311*, 1229−1233.

(35) Park, J.; Koo, B.; Hwang, Y.; Bae, C.; An, K.; Park, J.-G.; Park, H. M.; Hyeon, T. Novel Synthesis of Magnetic Fe_2P Nanorods from Thermal Decomposition of Continuously Delivered Precursors Using a Syringe Pump. *Angew. Chem.* **2004**, *116*, 2332−2335.

(36) Chen, J.-H.; Tai, M.-F.; Chi, K.-M. Catalytic Synthesis, Characterization and Magnetic Properties of Iron Phosphide Nanowires. *J. Mater. Chem.* **2004**, *14*, 296−298.

DOI: 10.1021/acsomega.8b00482
ACS Omega 2018, 3, 7655−7662

(37) Henkes, A. E.; Schaak, R. E. Trioctylphosphine: A General Phosphorus Source for the Low-Temperature Conversion of Metals into Metal Phosphides. *Chem. Mater.* **2007**, *19*, 4234−4242.
(38) Ponrouch, A.; Taberna, P.-L.; Simon, P.; Palacín, M. R. On the Origin of the Extra Capacity at Low Potential in Materials for Li Batteries Reacting Through Conversion Reaction. *Electrochim. Acta* **2012**, *61*, 13−18.
(39) Jiang, Y.; Zhang, D.; Li, Y.; Yuan, T.; Bahlawane, N.; Liang, C.; Sun, W.; Lu, Y.; Yan, M. Amorphous Fe2O3 as a high-capacity, high-rate and long-life anode material for lithium ion batteries. *Nano Energy* **2014**, *4*, 23−30.
(40) Park, C.-K.; Park, S.-B.; Shin, H.-C.; Cho, W.-I.; Jang, H. Li Ion Diffusivity and Rate Performance of the LiFePO4 Modified by Cr Doping. *Bull. Korean Chem. Soc.* **2011**, *32*, 191−195.
(41) Xiong, H.; Slater, M. D.; Balasubramanian, M.; Johnson, C. S.; Rajh, T. Amorphous TiO2 Nanotube Anode for Rechargeable Sodium Ion Batteries. *J. Phys. Chem. Lett.* **2011**, *2*, 2560−2565.
(42) Heitjans, P.; Tobschall, E.; Wilkening, M. Ion transport and diffusion in nanocrystalline and glassy ceramics. *Eur. Phys. J.: Spec. Top.* **2008**, *161*, 97−108.
(43) Larcher, D.; Beattie, S.; Morcrette, M.; Edström, K.; Jumas, J.-C.; Tarascon, J.-M. Recent Findings and Prospects in the Field of Pure Metals as Negative Electrodes for Li-Ion Batteries. *J. Mater. Chem.* **2007**, *17*, 3759−3772.
(44) Sauvage, F.; Tarascon, J.-M.; Baudrin, E. In Situ Measurements of Li Ion Battery Electrode Material Conductivity: Application to Li_xCoO_2 and Conversion Reactions. *J. Phys. Chem. C* **2007**, *111*, 9624−9630.
(45) Kim, H.; Seo, M.; Park, M.-H.; Cho, J. A Critical Size of Silicon Nano-anodes for Lithium Rechargeable Batteries. *Angew. Chem., Int. Ed.* **2010**, *49*, 2146−2149.
(46) Lu, Y.; Tu, J. P.; Xiang, Y. J.; Wang, X. L.; Zhang, J.; Mai, Y. J.; Mao, S. X. Improved Electrochemical Performance of Self-assembled Hierarchical Nanostructured Nickel Phosphide as a Negative Electrode for Lithium Ion Batteries. *J. Phys. Chem. C* **2011**, *115*, 23760−23767.
(47) Lu, Y.; Tu, J.; Xiong, Q.; Qiao, Y.; Zhang, J.; Gu, C.; Wang, X.; Mao, S. X. Carbon-Decorated Single-Crystalline Ni_2P Nanotubes Derived from Ni Nanowire Templates: A High-Performance Material for Li-Ion Batteries. *Chem.—Eur. J.* **2012**, *18*, 6031−6038.
(48) Lu, Y.; Tu, J.-p.; Xiong, Q.-q.; Zhang, H.; Gu, C.-d.; Wang, X.-l.; Mao, S. X. Large-scale synthesis of porous Ni_2P nanosheets for lithium secondary batteries. *CrystEngComm* **2012**, *14*, 8633−8641.
(49) Dibden, J. W.; Meddings, N.; Owen, J. R.; Garcia-Araez, N. Quantitative Galvanostatic Intermittent Titration Technique for the Analysis of a Model System with Applications in Lithium−Sulfur Batteries. *ChemElectroChem* **2018**, *5*, 445−454.
(50) Kim, C.; Kim, J. W.; Kim, H.; Kim, D. H.; Choi, C.; Jung, Y. S.; Park, J. Graphene Oxide Assisted Synthesis of Self-assembled Zinc Oxide for Lithium-Ion Battery Anode. *Chem. Mater.* **2016**, *28*, 8498−8503.

DOI: 10.1021/acsomega.8b00482
ACS Omega 2018, 3, 7655−7662